Agricultural Journal 13 (5-6): 98-106, 2018
ISSN: 1816-9155

Chatter Instability Prediction of Ball-End Milling in Discrete Time Domain

[1]Babak Fadaei and [2]Hossein Pourbashash
[1]Adiban Institute of Higher Education, Department of Mechanical Engineering,
Faculty of Mechanics, Garmsar, Iran
[2]Department of Mathematics, University of Garmsar, Garmsar, Semnan, Iran

Abstract: This study describes a theoretical model for prediction of chatter vibration in ball end milling of flat surfaces using discrete time domain approach. A model is developed for dynamic cutting process which takes into consideration the variation of helix angle of the ball end mill along the cutting edge. The vibration of the tool is calculated by using a lumped-parameter model with two degrees of freedom. Expressions are based on the dynamics of ball end milling with regeneration in the uncut chip thickness. The dynamic cutting force coefficients are derived from orthogonal cutting data base using oblique transformation method and the dynamic parameters of cutting process such as shear stress, friction angle and shear angle due to variation in spindle speed and feed rate are considered. An update semi-discretization method is used to produce stability lobes. When the process is highly intermittent which occurs at high speeds and low radial depth of cuts, the stability lobes are more accurately solved by semi-discretization method. The chatter stability limit is indicated by the critical nominal depth of cut. The stability lobes agree well with the analytical method, the computationally expensive and complex numerical time domain simulations.

Key words: Chatter, ball end milling, dynamic cutting force, milling stability, semi discretization, stability

INTRODUCTION

Ball-end milling is one of the most widely used cutting processes in the automotive, aerospace, die/mold and machine parts industries, to maximize the productivity in a machining process, both the speed at which the tools can machine without causing deterioration in the system stability and accurate evaluations of machining stability are crucial. The cutting process is given a great deal of weight in the development and production of products. Therefore, reducing the time required for the cutting process is one of the most effective methods of achieving rapid product development and improving productivity. The cutting speed must be increased to reduce the machining time but this can provoke abnormal tool behavior such as chatter. Chatter vibration in machining operations usually has undesirable effects such as accelerated tool wear, excessive noise, damage of the machine tool, poor surface finish and low dimensional accuracy of the machined part. A commonly used method for avoiding chatter vibrations in machining is to select low spindle speeds and small depths of cut. However, using this method for chatter-free machining results in low productivity. Therefore, in order to maximize productivity, prediction of chatter vibration is essential. The theory of chatter vibration for single point cutting tools has been discussed by several researchers, for example, Koenigsberger and Tlusty (1970) and Merritt (1965). This theory is applicable in operations such as turning where the directions of the cutting forces can be considered to be time invariant. It is, however, difficult to apply it to a milling process, due to the variation of uncut chip thickness and cutting force vector with spindle rotation. Nevertheless the theory can be used for rough estimation of stability limits in milling, so that, the apparently stable conditions can be identified prior to carrying out a more accurate numerical computation, thereby reducing the computation time (Tsai *et al*., 1990).

Recently, various models for the prediction of chatter in end milling and face milling have been proposed (Smith and Tlusty, 1993; Tlusty and Ismail, 1981). An attempt to extend the application of these models to ball end milling, however, presents some difficulties. This is because in ball end milling, the cutting speed, helix angle and consequently, the effective rake angle vary along the cutting edge. Little work has been reported on chatter vibration in ball end milling (Abrari *et al*., 1998; Altyntas *et al*., 1999). In Ahmadi and Ismail (2012) the researchers of the current study developed the stability lobes in milling by including process damping in the formulation of the Semi Discretization Method (SDM).

Corresponding Author: Babak Fadaei, Adiban Institute of Higher Education, Department of Mechanical Engineering, Faculty of Mechanics, Garmsar, Iran

This study presents a predictive time-domain chatter model to produce stability lobe diagrams using an update semi-discretization method (Insperger and Stepan, 2004) introduced for delay differential equations. So, it is assumed that the vibration ball end tool is a system with two modes of vibration in two mutually perpendicular directions: the x and y-axes. The equations of motion for the system are solved by semi-discretization method and asymptotic stability trends are then examined for several up-milling, down-milling, radial immersions and helix angles milling. Finally a series of experimental validation tests are performed to discuss the conclusions from this researchers.

MATERIALS AND METHODS

Dynamic modeling

Vibration model of ball end milling: The vibration model of a milling system can be reduced to 2-DOF vibration system in the two orthogonal directions (Altintas and Budak, 1995). The equations of motion for the system are:

$$m_x\ddot{x}+c_x\dot{x}+k_x x = F_x \quad (1)$$

$$m_y\ddot{y}+c_y\dot{y}+k_y y = F_y \quad (2)$$

Where:

- m_x = The modal masses of the tool
- C_x and C_y = The modal damping constants of the tool
- k_x and k_y = The modal spring constants of the tool
- F_x and F_y = The cutting forces acting on the tool in the directions of the x and y axes, respectively

Geometric modeling of ball end milling: Sadeghi *et al.* (2000) introduced a force model using orthogonal cutting data for cutting inclined plan. The helical flutes were divided into M small differential oblique cutting-edge segments. The orthogonal cutting parameters are carried to oblique milling-edge geometry using the classical oblique transformation method. As shown in Fig . 1. In the ball end mill tool the cutter radius in the x-y plane at axial location z is:

$$M = \text{round}\left(\frac{\text{Upper-Axial}}{dz}\right), R(z) = \sqrt{R^2-(R-z)^2} \quad (3)$$

For an element at axial location z:

$$\sin(\theta_z) = \frac{z\tan(i_0)}{R(z)} \quad (4)$$

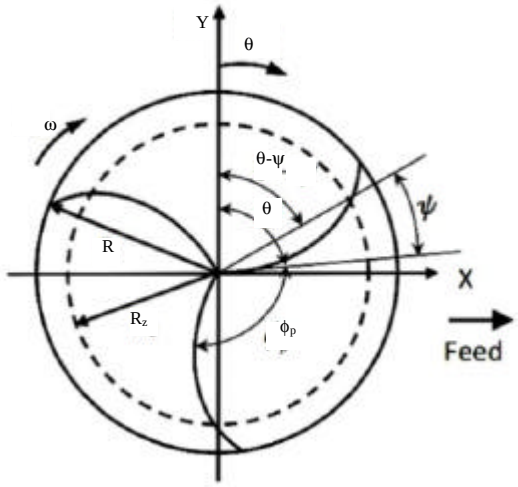

Fig. 1: Flute element position angle

where, θ_z is the angle between the ball tip z = 0 and an element at axial location z. It is measured clockwise from the z-axis vector from the Cartesian coordinate center to a point on the cutting edge and is defined by Naserian *et al.* (2007):

$$r = R(z)\sin(\theta_z)i+R(z)\cos(\theta_z)j+zk \quad (5)$$

Using Eq. 4 and 5:

$$r = z\tan(i_0)-\sqrt{R(z)^2-(z\tan(i_0))^2}\,j+zk \quad (6)$$

Thus:

$$dr = \left(\tan(i_0)i-\frac{R(z)\frac{dR(z)}{dz}-z\tan^2(i_0)}{\sqrt{R(z)^2-(z\tan(i_0))^2}}j+k\right)dz \quad (7)$$

The length of infinitesimal curved cutting edge segment d_s is computed from:

$$ds = \|dr\| = dz\sqrt{(\tan^2(i_0)-\left(\frac{R(z)\frac{dR(z)}{dz}-z\tan^2(i_0)}{\sqrt{R(z)^2-(z\tan(i_0))^2}}\right)^2+1}dz \quad (8)$$

Where:

$$\frac{dR(z)}{dz} = \frac{R-z}{R(z)} \quad (9)$$

And for the local helix angle:

$$\sin(i_z)ds = R(z)d\theta \quad (10)$$

Using Eq. 4:

$$d\theta = \frac{\tan(i_0)(R(z)-z\frac{dR(z)}{dz})}{R(z)\sqrt{R^2(z)-(z\tan(i_0))^2}}dz \quad (11)$$

And therefore:

$$i_z = \frac{R(z)d\theta}{ds} \quad (12)$$

Utilizing the Stabler's chip flow rule (i.e., $h_c = i$), the effective rake angle, α_e can be calculated from the following equation (Lee and Altintas, 1996):

$$\sin(\alpha_e) = \cos(i_z)\cos(\eta_c)\sin(\alpha_n)+\sin(\eta_c)\sin(i_z) \quad (13)$$

where, α_n and α_c are the normal rake angle and the chip flow angle, respectively. A point on the flute j at height z is defined by its angular position $\psi(j, q, z)$ on the global coordinate system:

$$\Psi(j,\theta,z) = \theta+(j-1)\frac{2\pi}{N}-(\theta_0-\theta_z) \quad (14)$$

where, θ is the tool rotation angle about z-axis and θ_0 is maximum angle between ball tip z = 0 and an element at axial location R and from Eq. 4:1

$$?_0 = \text{Arcsin}(\tan(i_0)) \quad (15)$$

Undeformed dynamic radial chip thickness: Radial chip thickness for static milling process with horizontal feed directions have been studied by Martelotti (1941) Martellotti (1945). In dynamic milling process, the cutting forces cause both the cutter and the workpiece to vibrate on the cutting surface. Each vibrating cutting tooth removes the wavy surface left by the previous tooth resulting in modulated chip thickness which can be expressed as:

$$h(\Psi_{j,\theta,z}) = f_t.\sin\Psi_{(j,\theta,z)}+(v_{j,0}-v_j) \quad (16)$$

where, F_t is the feed rate per flute, θ_j the angular immersion of the tooth j, υ_j , $\upsilon_{j,0}$ are the dynamic displacements due to the tool and workpiece vibration for the current and the previous tooth passing period. For the case of 3-axis dynamic ball-end milling, assuming circular tooth path and using Eq. 14:

$$h(\Psi_{j,\theta,z}) = [f_t.\sin\Psi_{j,\theta,z}+\Delta x\sin\Psi_{j,\theta,z}+ \Delta y\cos\Psi_{j,\theta,z}] \quad (17)$$

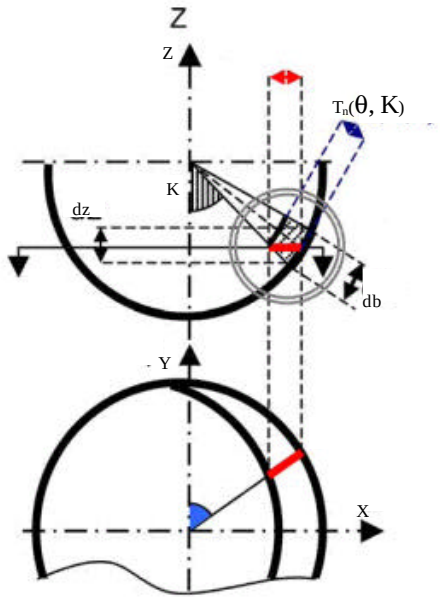

Fig. 2: Radial undeformed chip thickness (Lamikiz *et al*., 2004)

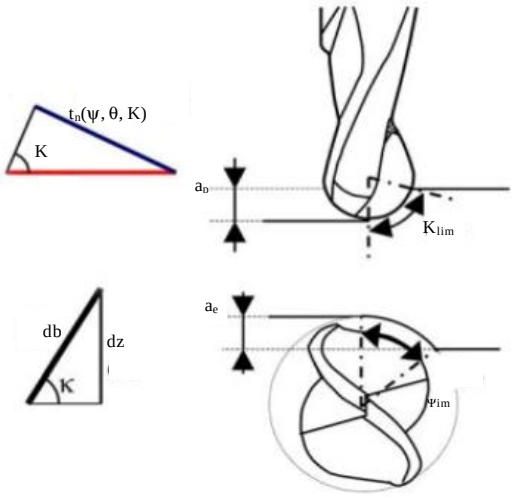

Fig. 3: Immersion geometry (Lamikiz *et al*., 2004)

$$\Delta x = x-x_{j,0}, \Delta y = y-y_{j,0} \quad (18)$$

as shown in Fig. 2. Radial chip thickness is equal to:

$$t_n(\Psi_{j,\theta,z}) = h(\Psi_{j,\theta,z})*\sin k \quad (19)$$

It is necessary to establish the engagement of the discrete element in part material as a constraint for each instant position. Therefore, the angles ψ_{lim} and k_{lim} determine the area where material is present in Fig. 3:

$$\text{if}\begin{cases}0\le k\le K_{lim}\\ 0\le \Psi\le \Psi_{lim}\end{cases}\rightarrow g(\Psi_{j,\theta,z})=1$$
$$\text{if}\begin{cases}k\ge K_{lim}\\ \Psi\ge \Psi_{lim}\end{cases}\rightarrow g(\Psi_{j,\theta,z})=0 \quad (20)$$

Where:

$$\Psi_{lim}=\cos^{-1}\left(\frac{R_0-a_e}{R_0}\right) \quad (21)$$

For the given angular position θ_j of the tool, the dynamic displacements of the cutter and the workpiece can be expressed in the fixed coordinate system as:

$$v_j = x\sin\theta_j + y\cos\theta_j \quad (22)$$

Usually, $\upsilon_{j,0}$ is modulated by the previous tooth (j-1) However, this is not always the case because the amplitude of oscillation might be large enough to make the tooth (j-1) lose contact with the surface being machined and then is outer modulated by $\upsilon_{j,0}$ the tooth (j-2) or even by the teeth (j-3), (j-4), etc. This is the basic nonlinearity of the dynamic milling process. This is the basic nonlinearity of the dynamic milling process.

Determining the specific cutting force coefficients: The cuting coefficients K_{tc}, K_{rc}, K_{ac} are identified from a set of orthogonal cutting tests using oblique transformation method (Wang, 1988). These coefficients depend on the part material and the substrate, coating, rake angle and helix angle of the tool. The relationship among the coefficients and these parameters is very complex. Therefore, it is necessary to estimate both shear and edge specific cutting coefficients for each couple tool-material:

$$K_{tc}=\frac{\tau_s(\cos(\beta_n-\alpha_n)+\tan i\tan\eta\sin\beta_n)}{\sin\varphi_n\sqrt{\cos^2(\varphi_n+\beta_n-\alpha_n)+\tan^2\eta\sin^2\beta_n}}$$
$$K_{rc}=\frac{\tau_s\sin(\beta_n-\alpha_n)}{\sin\varphi_n\cos i\sqrt{\cos^2(\varphi_n+\beta_n-\alpha_n)+\tan^2\eta\sin^2\beta_n}}$$
$$K_{ac}=\frac{\tau_s(\cos(\beta_n-\alpha_n)\tan i-\tan\eta\sin\beta_n)}{\sin\varphi_n\sqrt{\cos^2(\varphi_n+\beta_n-\alpha_n)+\tan^2\eta\sin^2\beta_n}} \quad (23)$$

The shear and edge coefficients are determined from characterization tests using the measured cutting forces as input data. By applying an inverse method, the coefficients are obtained by least square adjustment. The characterization tests carried out have been horizontal slot milling test with different cutting conditions. The Shear stress (τ_s), friction angle β_n and shear angle φ_n in machining of 1045 steel with a HSS cutting tool such that: are modeled using the following equations (Wang, 1988):

$$\tau_s = (1.586(V_c f_t)^{-0.25}+670.73)$$
$$\varphi_c = 105.7(V_c f_t)^{0.5}+0.375\alpha_e+13.64$$
$$\beta_n = 48.4(V_c f_t)^{0.125}+28.586-\varphi_c+\alpha_e \quad (24)$$

where, V_c (m/sec) is the cutting speed in the shear plane, τ_s (N/mm^2) is the shear stress in the shear plane.

Prediction of milling forces: The tangential, radial and axial components of cutting force acting on each cutting edge elements of each flute are calculated as:

$$\begin{cases}dF_{t,j}=(K_{tc}t_n(\Psi_{j,\theta,z})db+K_{te}ds)g(\Psi_{j,\theta,z})\\ dF_{r,j}=(K_{rc}t_n(\Psi_{j,\theta,z})db+K_{re}ds)g(\Psi_{j,\theta,z})\\ dF_{a,j}=(K_{ac}t_n(\Psi_{j,\theta,z})db+K_{ae}ds)g(\Psi_{j,\theta,z})\end{cases} \quad (25)$$

where, dF_t, dF_r, dF_a (N) are tangential, radial, axial cutting force components, respectively, K_{tc}, K_{rc}, K_{ac} (N/mm^2) are the specific coefficients K_{te}, K_{re}, K_{ae} (N/mm) are the edge specific coefficients, ds is the length of each discrete elements of cutting edge, t_n (mm) is radial undeformed chip thickness and db (mm) is the chip width in each cutting edge discrete element (Fig. 3):

$$db=\frac{dz}{\sin k} \quad (26)$$

The differential cutting forces acting on flute's cutting edges of the ith element calculated using Eq. 24 transformed to Cartesian coordinates are as follows:

$$\begin{cases}dF_{x,i,j}=-dF_{r,j}\sin k\sin\Psi_{j,\theta,z}-dF_{t,j}\cos\Psi_{j,\theta,z}-\\ \qquad dF_{a,j}\cos k\sin\Psi_{j,\theta,z}\\ dF_{y,i,j}=+dF_{r,j}\sin k\cos\Psi_{j,\theta,z}-dF_{t,j}\sin\Psi_{j,\theta,z}-\\ \qquad dF_{a,j}\cos k\cos\Psi_{j,\theta,z}\end{cases} \quad (27)$$

By summing up these forces, the total cutting forces acting on each disk element will be calculated and we can calculate the cutting forces in any axial depth of cut a; by summing up these differential cutting forces acting on disk elements and an given axial depth of cut:

$$\begin{cases}dF_{x,i}=\sum_{j=1}^{N}dF_{x,i,j}\\ dF_{y,i}=\sum_{j=1}^{N}dF_{y,i,j}\end{cases}\rightarrow\begin{cases}F_{x,a}=\sum_{i=1}^{m}dF_{x,i}\\ F_{y,a}=\sum_{i=1}^{m}dF_{y,i}\end{cases} \quad (28)$$

where, a (mm) is the instantaneous axial depth of cut and 0 ≤a≤ Upper axial, 1≤m≤M is the integer number of the elements in axial depth of cut a. We can rewrite Eq. 28 to form:

$$\begin{bmatrix} F_{x,a} \\ F_{y,a} \end{bmatrix} = \left[A_{a,\theta}\right] \cdot \begin{bmatrix} f_t + \Delta x \\ \Delta y \end{bmatrix} \tag{29}$$

F_t doesn't any contribution on stability and will be neglected, $[A_{a,\theta}]$ is square matrix and define as:

$$\begin{bmatrix} A_{xx} & A_{xy} \\ A_{yx} & A_{yy} \end{bmatrix}_{a,\theta} = \left[A_{a,\theta}\right] \tag{30}$$

The elements of $\begin{bmatrix} A_{xx} & A_{xy} \\ A_{yx} & A_{yy} \end{bmatrix}_{a,\theta}$ expressed as:

$$\begin{aligned}
A_{xx}^{a,\theta} &= \sum_{i=1}^{m}\sum_{j=1}^{N}\left(\begin{matrix}-K_{rc}\sin^2\Psi\sin k - K_{tc}\sin\Psi\cos\Psi - \\ K_{ac}\sin\Psi\sin k\cos k\end{matrix}\right)g_\Psi dz \\
A_{xy}^{a,\theta} &= \sum_{i=1}^{m}\sum_{j=1}^{N}\left(\begin{matrix}-K_{rc}\sin\Psi\cos\Psi\sin k - K_{tc}\cos^2\Psi - \\ K_{ac}\sin\Psi\cos\Psi\cos k\end{matrix}\right)g_\Psi dz \\
A_{yx}^{a,\theta} &= \sum_{i=1}^{m}\sum_{j=1}^{N}\left(\begin{matrix}-K_{rc}\sin\Psi\cos\Psi\sin k + K_{tc}\sin^2\Psi - \\ K_{ac}\sin\Psi\cos\Psi\cos(k)\end{matrix}\right)g_\Psi dz \\
A_{yy}^{a,\theta} &= \sum_{i=1}^{m}\sum_{j=1}^{N}\left(\begin{matrix}-K_{rc}\cos^2\Psi\sin k + K_{tc}\sin\Psi\cos\Psi - \\ K_{ac}\cos^2\Psi\sin k\end{matrix}\right)g_\Psi dz
\end{aligned} \tag{31}$$

now rewrite Eq. 1, 2:

$$\begin{cases} m_x\ddot{x}+c_x\dot{x}+k_x x = A_{xx}(x(t)-x(t-T)) + \\ \qquad A_{xy}\Delta y(y(t)-y(t-T)) \\ m_y\ddot{y}+c_y\dot{y}+k_y y = A_{yx}(x(t)-x(t-T)) + \\ \qquad A_{yy}\Delta y(y(t)-y(t-T)) \end{cases} \tag{32}$$

Or:

$$\begin{aligned}
&\begin{pmatrix}\ddot{x}(t)\\ \ddot{y}(t)\end{pmatrix} + \begin{pmatrix}2\zeta\omega_{nx} & 0\\ 0 & 2\zeta\omega_{ny}\end{pmatrix}\begin{pmatrix}\dot{x}(t)\\ \dot{y}(t)\end{pmatrix} + \\
&\begin{pmatrix}\omega_{nx}^2+\dfrac{A_{xx}^{a,\theta}}{m_x} & \dfrac{A_{xy}^{a,\theta}}{m_x}\\ \dfrac{A_{yx}^{a,\theta}}{m_y} & \omega_{ny}^2+\dfrac{A_{yy}^{a,\theta}}{m_y}\end{pmatrix}\begin{pmatrix}x(t)\\ y(t)\end{pmatrix} = \\
&\begin{pmatrix}\dfrac{A_{xx}^{a,\theta}}{m_x} & \dfrac{A_{xy}^{a,\theta}}{m_x}\\ \dfrac{A_{yx}^{a,\theta}}{m_y} & \dfrac{A_{yy}^{a,\theta}}{m_y}\end{pmatrix}\begin{pmatrix}x(t-T)\\ y(t-T)\end{pmatrix}
\end{aligned} \tag{33}$$

Semi-Discretization Method (SMD): The basic idea of the semi discretization method is to discretize the delayed terms of the Delay Differential Equation (DDE) while leaving the current time terms unchanged. This way, the DDE is approximated by a series of Ordinary Differential Equations (ODEs) for which the solutions are known and can be given in closed form. The governing equation of milling in Eq. 33 is a delayed differential equation with the tooth passing period as delay. to simplify the notation, Eq. 36 may be rewritten as:

$$\dot{u}(t) = A.u(t)+B.u(t-T) \tag{34}$$

Where:

$$A = \begin{pmatrix} 0 & 0 & 1 & 1 \\ 0 & 0 & 0 & 1 \\ -\omega_{nx}^2+\dfrac{.A_{xx}}{m_x} & \dfrac{.A_{xy}}{m_x} & -2\zeta\omega_{nx} & 0 \\ \dfrac{w.A_{yx}}{m_y} & -\omega_{nx}^2+\dfrac{.A_{yy}}{m_y} & 0 & -2\zeta\omega_{ny} \end{pmatrix},$$

$$B = \begin{pmatrix} 0 & 0 & 0 & 0 \\ 0 & 0 & 0 & 0 \\ -\dfrac{.A_{xx}}{m_x} & -\dfrac{A_{xy}}{m_x} & 0 & 0 \\ -\dfrac{.A_{yx}}{m_y} & -\dfrac{.A_{yy}}{m_y} & 0 & 0 \end{pmatrix}, u(t) = \begin{pmatrix} x(t) \\ y(t) \\ \dot{x}(t) \\ \dot{y}(t) \end{pmatrix} \tag{35}$$

Discretization is introduced using a time interval $[t_i, t_{i+1}]$ with $t_{i+1}-t_i = \Delta t$. The delay time becomes $T = (m+0.5)\,\Delta t$ where m is an integer determining the coarseness of the discretization. The periodic coefficients $A(t) = A(t+T)$, $B(t) = B(t+T)$ and in the i th semi-discretization interval, delayed state u(t-T) are approximated by:

$$\begin{aligned} &A(t) \approx A_i,\ B(t) \approx B_i \\ &u(t-T) \approx 0.5(u_{i-m+1}+u_{i-m}) \end{aligned} \tag{36}$$

The DDE in Eq. 34 is here with transformed into a series of autonomous second order ODEs with $t_i \le t \le t_{i+1}$ which can be rewritten as systems of first order ODEs:

$$\dot{u}(t) = A_i u(t) + \frac{B_i}{2}(u_{i-m+3}+u_{i-m}) \tag{37}$$

for the initial condition $u(t_i) = u_i$ and substituting $t = t_i$ and $u_{i+1} = u(t_{i+1})$ into this solution the solution is determined as:

$$u_{i+1} = P_i u_i + \frac{R_i}{2}(u_{i-m+3}+u_{i-m}) \tag{38}$$

where:

$$P_i = \exp(A_i\Delta t), R_i(A_i\Delta t)\text{-}A_i^{-1}B_i \quad (39)$$

Equation 39 can be rewritten as a map $Z_{i+1} = D_iZ_i$, with the state vector Z_i and the coefficient matrix D_i:

$$Z_i = \text{col}(x_i \quad y_i \quad \dot{x}_i \quad \dot{y}_i \quad x_{i-1} \quad y_{i-1} \quad ,\ldots, \quad x_{i-m} \quad y_{i-m}) \quad (40)$$

$$D_i = \begin{pmatrix} p_{i,11} & p_{i,12} & p_{i,13} & p_{i,14} & 0 & ,\ldots, & 0 & w_aR_{i,11} & w_aR_{i,12} & w_aR_{i,11} & w_aR_{i,12} \\ p_{i,21} & p_{i,22} & p_{i,23} & p_{i,24} & 0 & ,\ldots, & 0 & w_aR_{i,21} & w_aR_{i,22} & w_aR_{i,21} & w_aR_{i,22} \\ p_{i,31} & p_{i,32} & p_{i,33} & p_{i,34} & 0 & ,\ldots, & 0 & w_aR_{i,31} & w_aR_{i,32} & w_aR_{i,31} & w_aR_{i,32} \\ p_{i,41} & p_{i,42} & p_{i,43} & p_{i,44} & 0 & ,\ldots, & 0 & w_aR_{i,41} & w_aR_{i,42} & w_aR_{i,41} & w_aR_{i,42} \\ 1 & 0 & 0 & 0 & 0 & ,\ldots, & 0 & 0 & 0 & 0 & 0 \\ 0 & 1 & 0 & 0 & 0 & ,\ldots, & 0 & 0 & 0 & 0 & 0 \\ 0 & 0 & 0 & 1 & 0 & 0 & 0 & 0 & 0 & 0 & 0 \\ . & . & . & . & . & . & . & . & . & . & . \\ . & . & . & . & . & . & . & . & . & . & . \\ . & . & . & . & . & . & . & . & . & . & . \\ 0 & 0 & 0 & 0 & 0 & 0 & ,\ldots, & 0 & 0 & 0 & 0 \\ 0 & 0 & 0 & 0 & 0 & 0 & ,\ldots, & 1 & 0 & 0 & 0 \\ 0 & 0 & 0 & 0 & 0 & 0 & ,\ldots, & 0 & 1 & 0 & 0 \end{pmatrix} \quad (41)$$

The transition matrix over the principal period T is approximated by coupling the solutions of m successive intervals as:

$$\phi = D_{k-1}D_{k-2}, \ldots, D_1D_0 \quad (42)$$

Finally, stability of the investigated system is determined by the eigenvalues of the transition matrix ϕ. The system is stable if all eigenvalues of ϕ are in modulus less than one. Further details on the semi discretization procedure can be found in Insperger and Stepan (2004). In the case of milling, two possible instabilities can be observed.

The critical eigenvalue of ϕ is complex and its modulus is greater than 1. This case corresponds to the Hopf bifurcation causing the quasi periodic chatter (Mann *et al*., 2004).

The critical eigenvalue of f is real and its value is smaller than -1. This case corresponds to the period doubling or flip bifurcation which causes the periodic chatter.

These two instabilities are illustrated in Fig. 4 and 5 by the eigenvalue trajectories in the complex plane accompanied by the stability chart with the corresponding

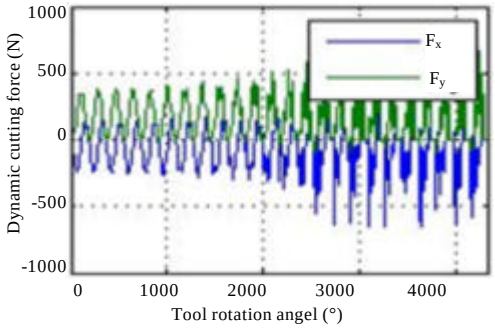

Fig. 4: Dynamic cutting force

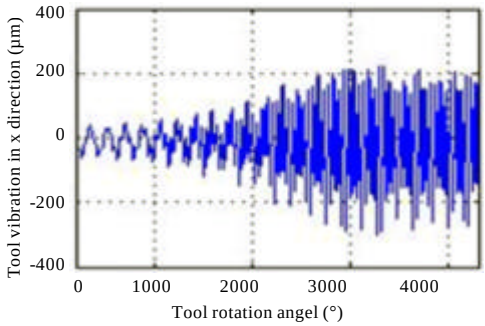

Fig. 5: Tool vibration in x-direction

depth of cut and spindle speed values. In the case of Hopf bifurcation, a pair of complex conjugate eigenvalues penetrates the unit circle in the complex plane whereas in the case of flip bifurcation, the unit circle is penetrated by one real and negative eigenvalue. More information on bifurcations in dynamical systems can be found in Wang (1988).

RESULTS AND DISCUSSION

Dynamic simulation results: The dynamic milling model has been implemented in "MATLAB". The input data to the program includes the cutter geometry, workpiece material and dimensions, cutting conditions (axial depth of cut, radial immersion, chip load, spindle speed), machine tool dynamics, cutting coefficients and other miscellaneous variables such as number of digitized points on the cut surface and simulation time step. Each simulation runs in a series of small time steps for the chosen duration. At each instant, the cutting forces and tool deflections are recomputed. The simulation program predicts dynamic milling forces, dynamic displacements of the ball milling tool at the tool tip in the x-y plane in any position of the cutting edge during cutting process. The milling force distributed non-uniformly along the edge for the special geometry of the ball part, the rotation of cutter

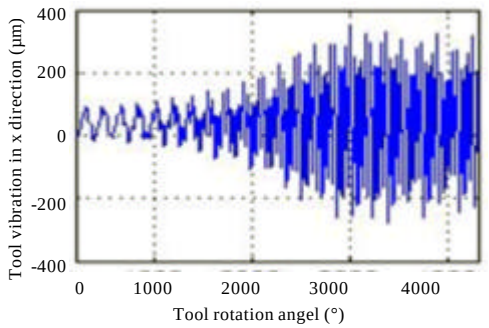

Fig. 6: Tool vibration in y-direction

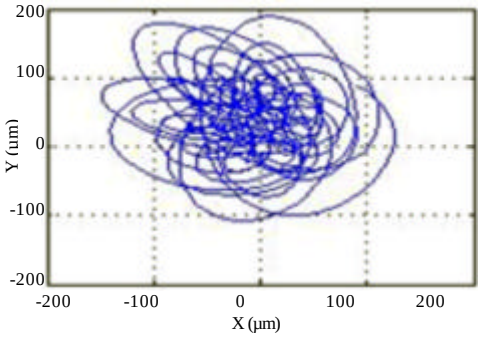

Fig. 7: Tooltip movement in xy-plane

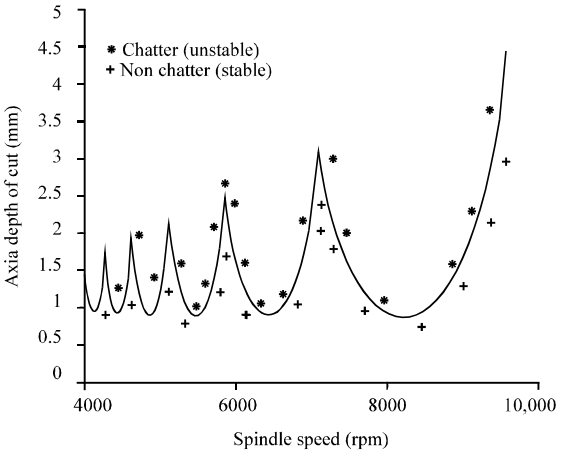

Fig. 8: Stability lobes and dynamic simulation; Ball-end, N = 2, Immersion 100%

and the different cutting depth. There are two typical states: the steady state (full immersion) and the transient state (cutting-in or exit) which can stand for the dynamics of the model for a ball-end milling cutter. The method used to calculate the runout parameters is derived from the basic concept that only one value of each cutting coefficient exists at a given instantaneous uncut chip thickness, regardless of the cutting conditions. Ideally, one should be able to calculate K_{tc}, K_{rc}, K_{ac} from the physical cutting force model and the synchronized measured cutting forces (Wang *et al*., 2015). However, the runout related parameters cause significant discrepancies. From the basic concepts described above, the runout parameters can be determined by choosing values that generate the minimum standard deviation of the cutting force coefficients at the given instantaneous uncut chip thickness in the physical cutting force model during one revolution of the cutter. The cutting force coefficients can then be determined by substituting the estimated runout parameters (Quintana and Ciurana, 2011).

For a set of milling with the ball-end-mill tool with the different cutting conditions and geometrical and dynamical parameters described in Fig. 4-8. We simulate the dynamical force. After many simulations we consider that the depth of cut and spindle speed are the main parameters that affect the dynamic force and tool vibration:

$$\text{Ball\_End,Down\_milling, Axial\_Depth} = 2(\text{mm}),$$
$$N = 2,\ n = 12000\ (\text{rpm}),$$
$$\text{helix} = 30^{\circ},\ \text{feed} = 0.05\left(\frac{\text{mm}}{\text{rev-tooth}}\right),\ R = 10\ (\text{mm}),$$
$$\text{immersion} = 100\%,\ \alpha_r = 12^{\circ},$$
$$\omega_{nx} = 675\ (\text{Hz}),\ \omega_{ny} = 660\ (\text{Hz}),\ m_x = 2.78,$$
$$m_y = 2.75\ (\text{kg}),\ \zeta_x = 0.0378,\ \zeta_y = 0.0365$$

The cutting force coefficients can then be determined by substituting the estimated runout parameters.

Stability lobe diagrams: In this study, dynamic stability of milling process with a ball-end mill tool has been investigated with the semi-discretization method. And the influence of effects of various parameters like cutting depth, spindle speed, number of tool flutes and the percent of tool immersion in the stability of process has been studied. In all cases, we assume that the tool helix angle = 30°, tool rake angle α_r = 12°, radius of the Ball-End tool R = 10 (mm), feed rate = 0.05 (mm/rev-tooth) and the dynamical coefficients of the machine tool in the x and y direction are ω_{nx} = 675 (Hz), ω_{ny} = 660 (Hz), m_x = 2.78 (kg), m_y = 2.75 (kg), ξ_x = 0.0378 (kg), ξ_y = 0.0365 (kg) (Grossi *et al*., 2015).

The effect of depth of cut: One of the most impressive parameters in the stability of the cutting process is the

depth of cut. It is seen from the stability lobe that in the low speeds of spindle when this parameter increases the chatter may occur but in the higher spindle speeds this parameter lonely has less affect on the chatter.

The effect of spindle speed: The revolution of spindle/min. describes the cutting speed and is the other important parameter for avoiding the chatter. From stability lobe diagram it is seen that in high speed of spindle with regulation of the cutting speed we have no chatter.

The effect of number of tool flutes: According to the most stability lobe diagrams derived by "MATLAB" program it can be seen that when this parameter increases, the distance between lobes will increase, the depth of cut for non chatter process will decrease and the probability of chatter occurring will be stronger.

The effect of immersion of tool: It is obviously seen from the drawn stability lobes that with increasing of the tool immersion, the safety depth of cut for avoiding the chatter will decrease.

Validate the stability lobe with dynamic simulation: For the many various depths of cut and spindle speed we solve the dynamical equation and compare them with the point on stability lobe to consider the validation of stability lobe diagram (Ma *et al*., 2016).

CONCLUSION

The stability lobe diagram that has been obtained from the semi-discretization method has a good agreement with the dynamical model, solved numerically. It considers that in low depth of cut the chatter will not occur and when the depth of cut increases, the chatter may occur But it is strongly dependent on the spindle speed and in the higher depth of cut with increasing the spindle speed we will avoid the chatter and have a stable cutting process.

REFERENCES

Abrari, F., M.A. Elbestawi and A.D. Spence, 1998. On the dynamics of ball end milling: Modeling of cutting forces and stability analysis. Intl. J. Mach. Tools Manuf., 38: 215-237.

Ahmadi, K. and F. Ismail, 2012. Investigation of finite amplitude stability due to process damping in milling. Procedia CIRP, 1: 60-65.

Altintas, Y. and E. Budak, 1995. Analytical prediction of stability lobes in milling. CIRP. Ann. Manuf. Technol., 44: 357-362.

Altyntas, Y., E. Shamoto, P. Lee and E. Budak, 1999. Analytical prediction of stability lobes in ball end milling. J. Manuf. Sci. Eng., 121: 586-592.

Grossi, N., A. Scippa, L. Sallese, R. Sato and G. Campatelli, 2015. Spindle speed ramp-up test: A novel experimental approach for chatter stability detection. Intl. J. Mach. Tools Manuf., 89: 221-230.

Insperger, T. and G. Stepan, 2004. Updated semi-discretization method for periodic delay-differential equations with discrete delay. Intl. J. Numer. Meth. Eng., 61: 117-141.

Koenigsberger, F. and J. Tlusty, 1970. Theory of Chatter Stability Analysis. In: Machine Tool Structures, Koenigsberger, F. and J. Tlusty (Eds.). Pergamon Press, Oxford, UK., pp: 145-163.

Lamikiz, A., L.N.L. de Lacalle, J.A. Sanchez and M.A. Salgado, 2004. Cutting force estimation in sculptured surface milling. Int. J. Mach. Tools Manuf., 44: 1511-1526.

Lee, P. and Y. Altintas, 1996. Prediction of ball-end milling forces from orthogonal cutting data. Intl. J. Mach. Tools Manuf., 36: 1059-1072.

Ma, Y., M. Wan and W. Zhang, 2016. Effect of cutter runout on chatter stability of milling process. Procedia CIRP, 56: 115-118.

Mann, B.P., P.V. Bayly, M.A. Davies and J.E. Halley, 2004. Limit cycles, bifurcations and accuracy of the milling process. J. Sound Vibr., 277: 31-48.

Martellotti, M.E., 1945. An analysis of the milling process part 2: Down milling. Trans. ASME., 67: 233-251.

Martelotti, M.E., 1941. An analysis of the milling process. Trans. ASME., 63: 677-700.

Merritt, H.E., 1965. Theory of self-excited machine-tool chatter: contribution to machine-tool chatter research. J. Eng. Ind., 87: 447-454.

Naserian, R.S., M.H. Sadeghi and H. Haghighat, 2007. Static rigid force model for 3-axis ball-end milling of sculptured surfaces. Intl. J. Mach. Tools Manuf., 47: 785-792.

Quintana, G. and J. Ciurana, 2011. Chatter in machining processes: A review. Intl. J. Mach. Tools Manuf., 51: 363-376.

Sadeghi, M.H., A.E. Amir and H.A. Haghighat, 2000. Modellinf of cutting forces in ball-end milling. J. Faculty Eng., 24: 39-48.

Smith, S. and J. Tlusty, 1993. Efficient simulation programs for chatter in milling. CIRP. Ann. Manuf. Technol., 42: 463-466.

Tlusty, J. and F. Ismail, 1981. Basic non-linearity in machining chatter. CIRP. Ann. Manuf. Technol., 30: 299-304.

Tsai, M.D., S. Takata, M. Inui, F. Kimura and T. Sata, 1990. Prediction of chatter vibration by means of a model-based cutting simulation system. CIRP. Ann. Manuf. Technol., 39: 447-450.

Wang, S.B., L. Geng, Y.F. Zhang, K. Liu and T.E. Ng, 2015. Cutting force prediction for five-axis ball-end milling considering cutter vibrations and run-out. Intl. J. Mech. Sci., 96: 206-215.

Wang, W.P., 1988. Application of solid modeling to automate machining parameters for complex parts. Manuf. Syst., 7: 57-63.